Induction of the nicotinamide riboside kinase NAD^+ salvage pathway in skeletal muscle of H6PDH KO mice

Craig L. Doig[1,2], Agnieszka E. Zelinska[1], Lucy A. Oakey[1,2], Rachel S. Fletcher[1,2], Yasir El Hassan[1,2], Antje Garten[1], David Cartwright[1,2], Silke Heising[1,2], Daniel A Tennant[1,2], David Watson[3], Jerzy Adamski[4] & Gareth G. Lavery[1,2].

[1]Institute of Metabolism and Systems Research, 2nd Floor IBR Tower, University of Birmingham, Birmingham, B15 2TT, UK. [2]Centre for Endocrinology, Diabetes and Metabolism, Birmingham Health Partners, Birmingham, B15 2TH. [3]Strathclyde Institute of Pharmacy and Medical Sciences, Hamnett Wing John Arbuthnott Building, Glasgow G4 0RE. [4]Helmholtz Zentrum Munchen GmbH, Ingolstadter Landstrasse 1, D-85764 Neuherberg. Germany.

Corresponding author:

Gareth G Lavery, PhD

Wellcome Trust Senior Research Fellow

Institute of Metabolism and Systems Research

University of Birmingham

Edgbaston

Birmingham, UK

B15 2TT

Tel: +44 121 414 3719 Fax: +44 121 415 8712

Email: g.g.lavery@bham.ac.uk

Disclosure statement: The authors have nothing to disclose.

Abbreviated title: NAD+ metabolism and ER stress in skeletal muscle myopathy

Word Count: 5504; 7 Figures (Inclusive of 3 Supplemental)

Abstract

Background: Hexose-6-Phosphate Dehydrogenase (H6PDH) is the only known generator of the pyridine nucleotide NADPH from $NADP^+$ in the Endoplasmic/Sarcoplasmic Reticulum (ER/SR). However, its ability to influence cell wide pyridine biosynthesis and metabolism is unclear.

Methods: Skeletal muscle from H6PDH Knockout mice (H6KO) and Wild type controls (WT) was subject to metabolomic assessment and pathway analysis. NAD boosting was performed through intraperitoneal injection of Nicotinamide Riboside (NR) (400mg/kg) twice daily for 4 days. Mice were culled and skeletal muscle tissue collected the next day. Double knockout mice were generated through to breeding of H6KO with NRK2 knockout mice. These mice were assessed for NAD levels and ER stress response.

Results: H6KO skeletal muscle shows significant changes in the pathway regulating NAD+ biosynthesis with the Nicotinamide Riboside Kinase 2 gene (NRK2) being the most elevated gene. Assessment of the metabolic impacts of this dysregulation showed decreases in mitochondrial respiration and Acylcarnitine metabolism. Pharmacologically boosting NAD+ levels with NR had no significant impact over ER stress or Acetyl-CoA metabolism. A duel H6-NRK2 KO mouse exhibited changes in NAD^+ levels but no overt change in metabolism compared to the H6KO mouse.

Conclusions: This work shows a relationship between ER/SR status and wider muscle cell metabolism. The utility of NAD^+ boosting to skeletal muscle is demonstrated however, it is also evident that the extent of cellular stress and/or REDOX status may overcome any beneficial impact.

Keywords: Hexose-6-Phosphate Dehydrogenase, Endoplasmic/Sarcoplasmic Reticulum, Skeletal muscle, Nicotinamide Riboside, Nicotinamide Adenine Dinucleotide

Background

A complete understanding of REDOX biology within the Sarcoplasmic/Endoplasmic Reticulum (SR/ER) and any influence over cellular metabolism is lacking. Hexose-6-phosphate dehydrogenase (H6PDH) is the only recorded generator of NADPH (from $NADP^+$) within this cellular compartment. This exclusivity ensures its importance to not only SR/ER REDOX control and coenzyme generation for pyridine nucleotides, but also implicates it into wider skeletal muscle homeostasis[1,2].

The pyridine Nicotinamide Adenine Dinucleotide (NAD^+) is a fundamental contributor to cellular REDOX maintenance and energetic utilisation[3,4]. The rate limiting nature of NAD^+ to biochemical reactions make it fundamental to energetic metabolism including mitochondrial fatty acid catabolism and ATP generation.

Pharmacologic augmentation of NAD^+ through the use of precursors such as Nicotinamide Riboside (NR) has shown restorative potential in NAD^+ based therapies using a variety of cell types and animal models with supportive human studies[5-10]. Recent studies back this, showing a loss of NAD^+ salvage function leads to progressive muscle degeneration and boosting of the nicotinamide salvaging pathways liberates skeletal muscles from some of the deleterious impacts of ageing, muscular dystrophy and high-fat diet phenotypes[10-13]. The phosphorylation of NR into nicotinamide mononucelotide (NMN) occurs through two nicotinamide riboside kinases (NRKs) NRK1 and NRK2. In many tissues NRK1 is the dominant and rate limiting source of NR phosphorylation[14]. However, in skeletal muscle NRK2 is highly expressed and recent data highlights its roles within myocyte physiology[8]. Biosynthetic salvage of nicotinamide mediated by NRK2 has only recently been identified as having relevance to skeletal muscle biology and its function within atrophic models, ER stress and REDOX dysfunction are unstudied.

Furthermore, maintenance of the Sarcoplasmic Reticulum (skeletal muscle only) SR/ER REDOX pyridine pools and its contribution to whole cell NAD^+ levels is unclear. Hexose-6-phosphate dehydrogenase (H6PD) converts glucose 6-phosphate (G6P) to 6-Phosphoglucogonate (6-PG) and 6-Phosphglucogonatelactonase (6-PGL). Within the

SR/ER H6PD generates the rate limiting cofactor for intracellular glucocorticoid activation by 11beta-hydroxysteroid dehydrogenase type 1 (HSD11b1)[15]. The knockout of H6PDH produces profound metabolic dysfunction, with glycogen storage shifts in liver accompanied by improved glucose sensitivity[16]. Adipose analysis of whole body H6PD KO mice revealed reduced adiposity and changes in lipolytic rates, suggesting that absence of H6PDH switches the direction with which HSD11b1 acts upon glucocorticoids[17]. Thus the action of H6PDH upon metabolism are multifaceted and tissue-specific. Skeletal muscle from H6PDH KO mice exhibits changes in REDOX balance of the ER/SR and inducing Unfolded Protein Response. This in-turn induces myofibre loss, vacuole formation and fibre type switching. Permutations extend to the cytosolic and nuclear environment shifting metabolic activity of purine biosyntheisis[18]. Given the importance of the SR/ER to skeletal muscle and H6PD being the only source of NADPH within the SR/ER there is potential for SR/ER pyridine metabolism may be shifted in ways that are not yet attributed to H6PD function. In this study, we examined H6PD as a regulator skeletal muscle metabolism through the conversion of $NADP^+$ to NADP(H), and how this impacts upon cellular processes extending beyond the SR/ER confined environment. These data show that H6PDH not only has implications for the biosynthetic processes governing NAD^+ generation but also impacts wider cellular pathways such as lipid homeostasis and mitochondrial fatty acid oxidation.

Here we explore the relationship between H6PDH and NRK2, attempting to boost skeletal muscle NAD^+ bioavailability with acute NR supplementation. In order to further understand dependence of SR/ER actions upon NRK2 mediated NAD^+ biosynthesis we generated a whole body double-knockout of H6PD and NRK2, exploring how ablation of NRK2 within H6PDH defunct skeletal muscle alters metabolic function and mitochondrial activity. Our work reveals previously unconsidered aspects of NAD^+ metabolism showing an ER sensing mechanism that up-regulates a skeletal muscle NAD^+ biosynthesis pathway in response to altered NADPH availability.

Materials and Methods

Animal care, Mouse strains, storage

C57/BL5J mice were group housed in a standard temperature (22°C) and humidity-controlled environment with 12:12-hour light:dark cycle. Nesting material was provided and mice had ad libitum access to water and standard chow. Mice were sacrificed using schedule one cervical dislocation and tissues were immediately. Collections were all performed at 10-11am. Intraperitoneal injections of Nicotinamide Riboside (400mg/kg) were given twice daily. (10am and 3pm) for 4 days before cervical dislocation and skeletal muscle bed collection on Day 5 (10am), tissues were flash frozen, fixed or for high resolution respirometry stored in BIOPS buffer. Heterozygotes of H6PD KO and NRK2 KO were breed to generate H6-NRK2 KO mice. Mice were utilised between 8-12 weeks of age. Experiments were consistent with current UK Home Office regulations in accordance with the UK Animals (Scientific procedures) Act 1986.

RNA extraction and qRT-PCR

Total RNA was extracted from skeletal muscle tissue using TRI-reagent (Invitrogen). RNA quality was determined by visualisation on a 1.5% agarose gel and quantity was measured by nanodrop absorbance at 260nm. Reverse transcription was conducted using 1µg RNA that was incubated with 250uM random hexamers, 5.5mM $MgCl_2$, 500uM dNTPs, 20units RNase inhibitor 63units multi-scribe reverse transcriptase and 1x reaction buffer. Reverse transcription was performed on a thermocycler set at the following conditions: 25°C 10minutes, 48°C for 30 minutes before the reaction was terminated by heating to 98°C for 5 minutes. cDNA levels were determined using an ABI7500 system (Applied Biosystems), reactions were conducted in a 384-well plate in single-plex format. Primers and probes were purchased as Assay on Demand (FAM) products (Applied Biosystems). Total reaction volumes used were 10ul containing Taqman Universal PCR mix (Applied Biosystems). All reactions were normalised to 18s rRNA (VIC) (Applied Biosystems). The real-time PCR reaction was performed at the following conditions: 95°C for 10 minutes then 40 cycles of

95°C for 15 seconds and 60°C for 1 minute. Data were collected as Ct values and used to obtain deltaCt (dCt) values and expressed as fold change ±standard error of the mean(SEM).

mtDNA Copy number

DNA was isolated using phenol-chloroform and washed in Ethanol before quantification using nanodrop. DNA from all samples was diluted to 50ng/µl and subject to real-time PCR using SYBRgreen master mix (Applied Biosystems) using the following primers specific for nuclear and mitochondrial DNA.

Nuclear DNA: TERT Forward CTAGCTCATGTGTCAAGACCCTCTT Reverse GCCAGCACGTTTCTCTCGTT, Mitochondrial DNA: DLOOP Forward AATCTACCATCCTCCGTGAAACC Reverse TCAGTTTAGCTACCCCCAAGTTTAA, ND4 Forward AACGGATCCACAGCCGTA Reverse AGTCCTCGGGCCATGATT.

Western Immunoblotting

Protein lysates were collected in RIPA buffer (50mmol/l Tris pH 7.4, 1% NP40, 0.25% sodium deoxycholate, 150mmol/l NaCl, 1mmol/l EDTA), protease & phosphatase inhibitor cocktail (Roche, Lewes, U.K.), stored at -80°C (>30 minutes), defrosted on ice and centrifuged at 4°C (10mins, 12000 rpm). The supernatant was recovered and total protein concentration was assessed by Bio-Rad assay. Total proteins were resolved on a 12% SDS-PAGE gel and transferred onto a nitrocellulose membrane. Primary antibodies; Anti-Goat H6PDH (in house), Anti-Mouse NAMPT (Bethyl A300-372A), Anti-Rabbit NRK1 (in house), Anti-Rabbit NRK2 (in house), Anti-Rabbit CHOP (Cell Signaling D46F1 5554), Total Lysine Ac (Cell Signaling 9441), Anti-Mouse Rodent OXPHOS Mitoprofile (Abcam ab110413), IDH2 K413ac (GeneTel AC0004), IDH2 Total (Abcam ab55271), H3K9ac (Cell Signaling 9649), H3K18ac (Cell Signaling 9675), ERO1a (Cell Signaling 3264), PDI (Cell Signaling 3501), alpha-Tubulin (Santa Cruz B-7 sc-5286). Secondary antibodies (Dako) anti-mouse, anti-goat and anti-rabbit conjugated with HRP added at a dilution of 1/10,000. Equal loading of protein

content was verified using alpha-tubulin as a housekeeping protein and bands visualised using ECL detection system (GE Healthcare, UK). Bands were measured using Image J densitometry, and normalised to those of loading control (alpha tubulin).

High Resolution Respirometry of permeabilised muscle fibres by Oroboros

Respirometry studies in fast (Extensor Digitorum Longus) and slow twitch (Soleus) skeletal muscle myofibres were performed using high-resolution respirometry (Oroboros Instruments, Innsbruck, Austria). Fresh skeletal muscle (5mg) was stored in ice-cold 2mls BIOPS buffer. Any connective tissue and adipose was discarded and 20µl of Saponin stock solution for permeabilisation of muscle fibres (5mg Saponin per ml BIOPS buffer) added. The samples were then incubated for 30 minutes at 4°C. Muscles were washed in Mir05 for 10 minutes at 4°C before drying on filter paper. Approximately 3mgs of muscle tissue was introduced into the chamber and left for >10 minutes to give a stable baseline signal, re-oxygenation occurred once O_2 concentration reached 250µM. Sequential addition of inhibitors and substrates occurred as per Oroboros Instruments specified protocol for fatty acid oxidation.

NAD^+ Quantification by Colorimetric Assay

NAD^+ was extracted from flash frozen skeletal muscle and NAD^+/NADH quantified using the NAD^+/NADH Assay kit (BioAssay Systems) according to the manufacturers instructions.

Unbiased Metabolomic measurement

20mg of skeletal muscle previously flash frozen tissue from Tibialis Anterior (TA) or Soleus (SOL) was placed in dry ice. Metabolites were extracted into 0.5ml of ice-cold LCMS grade methanol:acetonitrile:water (50:30:20). Samples were pulverised and stored at 4°C for 10 minutes before centrifugation at 0°C 1300rpm for 15 minutes. Supernatant was then transferred to HPLC vials ready for LC/MS analysis. To preclude variables introduces from preparing samples separately all samples were prepared simultaneously in a randomised order and re-randomised before injection in the LC/MS.

Biocrates Targeted Metabolite kit

Skeletal muscle (Quadriceps), liver and plasma were collected from WT and H6KO and WT littermates. Frozen tissue was homogenised in tubes containing ceramic beads of 1.4mm diameter using extraction solvents. The AbsoluteIDQ p150 kit (Biocrates Life Science AG, Austria) was prepared according to the manufacturers instructions. Briefly, 10µl of tissue extract being used for PITC-derivatisation of amino acids, extraction with organic solvent and liquid handling steps. Metabolites were quantified with a reference to appropriate internal standards using FIA-MS/MS on a 400 QTRAP instrument (AB Sciex, Germany) coupled to a HPLC Prominence (Shimadzu Deutschland GmbH, Germany). A total of 163 metabolites were measured and divided into 6 groups (Supplementary Table 1).

Metabolomic set enrichment analysis

We conducted metabolite set enrichment analysis using MetaboAnalyst[19,20]. Significantly dysregulated metabolites from the unbiased measurement in H6KO compared to WT muscle were uploaded to Metaboanalyst. These were processed with the over-representation analysis (ORA) algorithm and the metabolic pathway associated metabolite library set. This examines the group of metabolites using Fisher's exact test, calculating the probability of seeing a particular number of metabolites containing the biological pathway of interest in the list of metabolites.

Statistical Analysis

Students T-test or ANOVA statistical comparisons were used with the Graphpad Software Inc. Prism version 5. Data presented as mean ±SEM with statistical significance determined as *. $p<0.05$, **. $p<0.01$, ***. $p<0.001$. Unpaired T-Test compared treatments or genotypes. Statistical analysis derived from real-time PCR data was determined using dCt values throughout.

Results

Sarco/Endoplasmic confined H6PD knockout produces muscle wide metabolic alterations in Nicotinamide metabolism. The Sarcoplasmic/Endoplasmic Reticulum serves as a major calcium store, driving the contractile response and contributing towards REDOX homeostasis through the generation of NADPH by H6PD. Previously, studies show the ablation of H6PDH in conditional skeletal muscle and whole body models provoking a muscle myopathy driven by SR/ER stress and the unfolded protein response. Additionally, the physiological role of H6PD upon glucocorticoid metabolism have been characterised, further highlighting the importance of SR/ER REDOX to NADPH generation[15,18]. We subjected skeletal muscle extracted from WT and H6KO mice to an unbiased metabolomic screen to better understand the role H6PD plays in wider muscle cell metabolism and SR/ER REDOX maintenance. This unbiased metabolite profile shows significant differential abundance of metabolites in the H6KO muscle **(Supplementary Table 1)**. The N6,N6,N6.-Trimethyl-L-Lysine metabolite is a methylated derivative of the amino acid lysine, a constituent of nuclear histone proteins and a precursor to carnitine and fatty acid oxidation in the mitochondria. 3-Hydroxysebasicacid was also significantly elevated in the H6KO muscle, a metabolite elevated in the urine of humans with peroxisomal disorders and glycogen storage disease[21,22], signalling a defect in fatty acids synthesis and metabolic defects such as medium chain acyl-CoA dehydrogenase deficiency. Cis-5-Tetradecenoylcarnitine is a marker of long chain acyl-dehydrogenase (VLCAD) deficiency, alterations in metabolites regulating beta oxidation are contributory to skeletal muscle myopathy[23]. There are significant elevations in both the metabolite Nicotinamide Adenine Dinucleotide (NAD^+) and the methylated form of NAD^+, 1-methylnicotinamide. This dataset was subject to pathway analysis to reveal overrepresentation of metabolites that sharing a metabolic pathway. The most highly overrepresented pathways were nicotinamide and pyridine biosynthesis **(Figure 1A-B)**. Changes in NAD^+ availability to skeletal muscle profoundly impacts downstream reactions intrinsic to metabolic function and defects in NAD^+ homeostasis are contributory to disease development[24-26]. To gain further insight NAD^+ generation in relation to the H6KO

model we conducted quantification of NAD^+, NAD(H) and NAD(H)total abundance in WT and H6KO skeletal muscle. These data show no significant NAD^+ changes of H6KO in comparison to WT. NADH is significantly decreased in H6KO, however, measurement of total NAD(H) levels were indifferent to WT **(Figure 1E-H)**. Critical to cellular NAD^+ maintenance are the multiple salvage and biosynthetic enzymes culminating with NAD^+ formation. The schematic showing these routes indicates that combinatorial sources leading to NRK2 generates NMN from NR contributing towards cellular NAD^+, which is consumed by cellular reactions and the by-product NAM is salvaged and regenerated into usable NAD^+ **(Figure 1G)**. Real-time PCR analysis of these genes responsible for muscle NAD^+ biosynthesis and salvage demonstrates changes in both biosynthetic and NAD^+ phosphorylating genes **(Figure 1H)**. There is significant increase in the skeletal muscle restricted nicotinamide riboside kinase 2 gene (NRK2), whilst the constitutively expressed NRK1 and NAMPT are unchanged. Responsible for the phosphorylation of the NAD^+ precursor nicotinamide riboside into nicotinamide mononucleotide NRK2 has been shown to be elevated in a model of cardiomyopathy[7]. Significantly down regulated genes in the H6KO implicated in NAD^+ biosynthesis show reductions in levels of nmnat2 a key enzyme skeletal muscle conversion of NMN into NAD^+ (but no change in nmnat1), suggesting restriction of a rate limiting response to the upregulated NRK2, moderating NAD^+ levels. Downregulation of NAD kinase limits generation of $NADP^+$, (the rate limiting coenzyme for H6PD within the SR/ER). This indicates an adaptive response serving to prevent $NADP^+$ build up in response to H6PDH ablation. Purine Nucleoside Phosphorylase (PNP) (converts NR to NAM) and the NAD^+ utilising ADP-Ribosyltransferase (ART1) are both downregulated underlying the disturbance in NAD^+ metabolism driving the wider metabolic disturbances showed in the H6KO muscle. Protein measurement of both NRK1 and NRK2 revealed significant elevations in H6KO samples. The rate limiting enzyme for NAD^+ salvage NAMPT remained unchanged indicating that H6KO mouse muscle may have elevated capacity to generate NMN from NR, whilst the contribution from salvaged NAM remained unchanged **(Figure 1 I-**

K). This presents the opportunity to examine the biosynthetic contribution as part of an adaptive metabolic response to cellular stress.

H6KO skeletal muscle has reduced mitochondrial fatty acid oxidative capacity and widespread changes in acylcarnitines.

Elevations in NAD^+ and NMN concentrations within skeletal muscle have been identified as promoting mitochondrial function[27-29]. We therefore, challenged the potential of upregulated NRK2 in the H6KO model to impact mitochondrial respiration rates. Despite a lack of NAD^+ increase within the H6KO muscle we reasoned that flux of NAD^+ turnover may still be changed, and this may have implications for energetic utilisation of mitochondria. Therefore, to assess mitochondrial metabolic function we subjected permeabilised skeletal muscle fibres from both the Tibialis anterior (TA) and Soleus (SOL) muscle beds to high-resolution respirometery, exploiting mitochondria's fatty acid oxidative capacity. Measurement of the fast twitch TA muscle from H6KO mice shows a decreased ability to consume oxygen for energetic metabolism in the H6KO model **(Figure 2A)**. This defect was also apparent in slow twitch Soleus muscle from H6KO **(Figure 2B)**. This suggests H6KO ablation has a detrimental impact upon mitochondria and the elevations in NAD^+ biosynthesis measured in NRK2 increased abundance are ineffectual and their impact upon mitochondrial metabolism. These results show H6KO (fast and slow twitch) muscle has significantly decreased ability to utilise substrates for fatty acid beta-oxidation and overall respiratory capacity. To understand if these measurements are a measure of functionality and not mitochondrial abundance we examined mtDNA content in both WT and H6KO muscle and found them to be unchanged **(Figure 2C)**. Together these data demonstrate in addition to the SR/ER disturbances H6KO skeletal muscle there is a widespread inability to utilise sources of energy for cellular respiration rising from occlusion in the generation of pyridine nucleotide NADPH within the SR/ER. This leads to widespread physiological deficits in mitochondrial function without altering mitochondrial protein levels. Total protein measurement and quantification of mitochondrial respiratory complex subunits indicated no change in overall abundance of ATP generating complexes **(Figure 2D)**. Using a targeted

metabolomic analysis of acylcarnitines and other metabolites **(Supplementary Figure 2)** we find short-chain acylcarnitines (C2, C3, C4, C5, C6 & C10:1) were differentially upregulated in H6KO muscle tissue, the ratio of acetylcarnitine to free carnitine (C2:C0) was increased signifying elevations in even numbered fatty acids within the H6KO. Free-carnitine was not significantly different in H6KO versus WT tissue **(Figure 2E)**. To gain further insight and reconcile observed changes in myofibre carnitine composition and shifts in phospholipid species we used real-time qPCR to examine expression of genes integral to carnitine acylation, lipid mobilisation and fatty acid metabolism. H6KO tissue shows significant elevations in acss2, far1, acsl2, acaa2 and scd1 **(Figure 2F)**. A schematic of disrupted genes in H6KO critical to the generation of acylcarnitine and fatty acid esters, contributing towards mitochondrial B-oxidation **(Figure 2G)**. Protein lysates collected from H6KO muscle show increases in Isocytrate Dehydrogenase 2 (IDH2) acetylation and histone 3 lysine 9 and lysine 18 acetylation, reflecting fatty acid oxidation and acyl-CoA changes observed in the unbiased metabolome measurements and the targeted metabolic screen **(Figure 2H)**.

Boosting of NAD^+ with the precursor Nicotinamide Riboside has no influence metabolic composition of H6KO mouse skeletal muscle.

To establish the utilisation of NRK2 and their importance to skeletal muscle metabolic function we supplemented both WT and H6KO animals with the NAD^+ precursor Nicotinamide Riboside (400mg/kg twice daily over 4 consecutive days). With the hypothesis being intraperitoneal injection of NR would provide additional substrate for utilisation by elevated NRK2 in H6KO muscle. Thus exploiting the upregulated biosynthetic route to NAD^+ ultimately rescuing the defects in these mice. Quantification of NAD levels in the skeletal muscle of mice receiving i.p NR shows it was successful at enhancing NAD^+ levels recorded in both WT and H6KO samples when compared to their sham treated controls **(Figure 3 A-D)**. However, NADH was only successfully elevated by i.pNR in H6KO, WT trended upwards but failed to achieve significance. This potentially signifies that although H6PD is the sole source of NADPH in the SR/ER and despite the high abundance of SR/ER in skeletal muscle it may not be a significant contributor towards total myocellular NAD(H). These data

demonstrate i.p NR over an acute schedule (4 days) is successful and elevating cellular NAD^+ in both WT and H6KO metabolically challenged mice. However, NADH is only augmented in the H6KO model, reflecting the enhanced NAD^+ biosynthetic and salvage network identified in the unbiased metabolomic screen. Transcript analysis of genes integral to NAD biosynthesis and salvage showed a decrease in NRK2 in WT, not shown in H6KO. I.P NR was successful at increasing the expression of NMNAT1, NAMPT and NRK1 in H6KO muscle, responses not measured in WT cells and may reflect shifts in the biosynthetic generation of the H6KO model. Additionally, a lack of response from NRK2 in the H6KO may suggest NRK2 is transcript is functioning towards physiological capacity **(Figure 3E)**. Measurement of transcripts regulating Acyl-CoA and lipid metabolism enzymes contributing towards beta-oxidation reveals that NAD^+ boosting has no impact over their expression **(Figure 3F)**. This suggests that increased NAD^+ concentrations produced by i.p.NR have limited/no bearing upon the mitochondrial energy utilisation of NAD^+ flux within skeletal muscle of WT animals. Protein quantification of NAMPT and NRK2 showed no change in abundance in response to i.p.NR **(Figure 3G+H)**. In order to further asses the effect of NR in skeletal muscle of WT and H6KO muscle and challenge the elevated NRK2 levels in H6KO muscle we subjected samples to high resolution respirometry fatty acid oxidation protocols and found H6KO muscle +i.p NR is significantly reduced in its O2 flux measurements when compared to WT i.p NR. The i.p NR data sets were not significantly different from their sham treated genotype controls suggesting that although acute i.p NR does increase NAD^+ concentrations within muscle there is no measurable bearing upon mitochondrial O2 flux. Furthermore, in H6KO mice attempts to exploit increased NRK biosynthetic route through i.p NR, and NAD+ concentration elevation does not overcome the metabolic defects induced by H6PDH ablation **(Figure 3 I-J)**. The H6KO model exhibits extensive ER stress response and unfolded stress response. To understand any impact upon this protein lysates from muscle were probed for the ER stress response protein CHOP and the protein folding regulators ERO1a and PDI **(Figure 3K)**. From these data it is evident that the acute i.p NR protocol has no significant impact upon the protein expression, suggesting that benefits of NAD^+ boosting

in other cellular functions may not extend into the ER/SR of skeletal muscle. NAD^+ boosting as a strategy to increase availability of the rate-limiting factor for the sirtuin enzyme family has shown some promising outcomes. Therefore, to assess acetylation levels changes in response to acute i.p NR in both WT and H6KO muscle protein lysates from these mice were examined for global acetylation and acetylation of the mitochondrial enzyme IDH2. These data show there was no change in acetylation status shown when compared to sham controls **(Figure 3L)**.

Ablation of NRK2 within the H6KO muscle decreases NAD^+ levels and is independent to the H6KO skeletal muscle myopathy.

As boosting of NAD^+ did not change the mitochondrial function or ER/SR stress status of the H6KO muscle we investigated the potential to perturb the H6KO induced NRK2 response. With our hypothesis stating NRK2 as being a dominant muscle NAD^+ contributing pathway crucial to whole cell pyridine levels. To challenge this we produced a double knockout model, deficient in both H6PD and NRK2. As NRK2 is skeletal muscle restricted, we reasoned that its ablation in the H6KO would negatively affect cellular NAD^+ content, exacerbating the H6KO muscle myopathy phenotype. Quantification of NAD^+ levels revealed that the Double knockout TA has significantly decreased NAD^+ and total NAD(H) total, indicating that the ablation of NRK2 in the H6 null muscle **(Figure 4A-D)**. H6KO skeletal muscle beds exhibit myopathy, this is reflected in the decreased muscle bed weights (**Figure 4 E-G)**. Assessment of NAD biosynthesis and salvage gene expression revealed no significant change in the DKO muscle compared to H6KO (NRK2 KO has no significant change compared to WT mice), suggesting that ablation of skeletal muscle restricted NRK2 can reduce the levels of NAD(H) generated but this may not affect cellular metabolic function **(Figure 4H)**. Quantitative real-time PCR of the fatty acids and Acyl-CoA genes upregulated in the H6 model have equivalent expression to DKO indicating no altered metabolic phenotype in the DKO muscle tissue. **(Figure 4I)**. Protein levels of the unfolded protein response is upregulated in the H6KO muscle and protein measurement of the DKO reflects an unchanged level of expression of the protein unfolded responses factors ERO1a and PDI.

These upregulated sensors of ER stress are not significantly altered in expression compared to H6KO suggesting NRK2 has little/no impact over the ability of the SR/ER UPR pathway **(Figure 4J+K)**.

Discussion

The SR/ER located H6PD is the only know source of NADPH within this largely impermeable compartment. Currently there is a gap in our understanding of how nucleotide pools independent to the cytosol (a high consumer of cellular NADPH with its own maintenance stores) relate to cellular pyridine homeostasis. We demonstrate that ER REDOX dysfunction perturbs mitochondrial lipid metabolism and cytosolic NRK2 mediated NAD^+ biosynthesis within skeletal muscle. The reduced bioenergetic capacity of H6KO mitochondria demonstrates that SR/ER stress signals confer extensive metabolic impairment. However, these direct signalling mechanism remains unresolved.

In contrast to H6KO conditional and global murine models that show a profound upregulation of the ER stress response human cancer cell lines of breast origin transient knockdown of H6PD produced a down regulation in ER stress[30]. Also reported was a reduction in migration and enhanced cell adhesion, these data suggest not only that cancer cells show reliance upon H6PD mediated NADPH generation for their proliferation but also that H6PD maybe a novel target. Importantly, supportive of our work this study in human cancer cells also demonstrated an increased mitochondrial superoxide levels, indicative of mitochondrial impairment. We demonstrate the SR/ER capability to create mitochondrial dysfunction, further quantifying the level of mitochondrial respirometry in H6PD defunct myofibres. Supportive of this notion is the identification of H6PD as a target of PARP inhibitor Rucaparib, (PARPs being NAD+ dependent enzymes) indicating current anti-cancer therapeutic strategies may already be exploiting the ability of the SR/ER to impact wider cell metabolism[31].

In an attempt to exploit enhanced NAD^+ biosynthetic enzyme expression in the H6KO skeletal muscle we delivered a saturated supply of high dose precursor, nicotinamide

riboside. This was successful at enhancing NAD^+ levels within the tissue, also it elevated NADH within H6KO samples. However, there was no change over the recorded metabolic features of the H6KO model with ER stress, acylation and mitochondrial fatty acid oxidation unchanged. Thus physiologically the elevation in NAD^+ was unable to overcome the negative attributes of H6PD ablation. The acute nature of the supply of NR (4 days) maybe considered a limitation of the study, with this duration it is unlikely that structural aberrations induced by the H6KO might be rescued. However, the acute delivery of NR did induce NAD sifts recorded within skeletal muscle in addition to regulatory changes in genes important to NAD^+ utilisation and salvage.

As an alternative strategy to challenge the relationship between NAD^+ biosynthesis and the SR/ER REDOX enzyme H6PD we produced a duel-knockout model with ablated H6PD-NRK2. This model exhibited a level of skeletal muscle myopathy comparable to the H6KO that was not exacerbated or rescued by the lack of NRK2 gene product. These data suggest generation of NADPH within the SR/ER by H6PD is essential to cellular metabolic functions external to the SR/ER environment. Differential NAD^+ homeostasis has been demonstrated to be present in muscular pathologies such as muscular dystrophy and infantile onset Pompe disease[32,33]. The latter being a glycogen storage disease and reflective of the H6PD glycogen storage defects[34]. Also in cardiac muscle it has been demonstrated that upregulation of NRK2 occurs as a response to congestive heart failure[7]. Herein we detail a similar mechanism for skeletal muscle with enhanced expression of NRK2 mRNA and protein indicating that this is an adaptive response and occurs independently of NAMPT activity. Attempting to delineate the NAD^+ biosynthetic changes introduced by H6PD showed although there was significant elevations in NRK2 mediated expression its NAD^+ generating contribution is presumably attenuated by the unchanged expression levels of the rate limiting NMNAT enzymes. Furthermore, the increase of NRKs (in particular NRK2) maybe an attempt to rectify the REDOX alteration within the H6PD KO SR/ER. Should this notion be confirmed would support the concept of organelle sensing and exchange of nucleotides, an attribute whose existence remains unclear partly due to a lack of identified transporters for

pyridine nucleotides. However, recent published data support the existence of mitochondrial membrane transporters able to distribute pyridine nucleotides between cytosolic and mitochondria, indeed the compartmentalisation of NAD^+ as a cellular mechanism capable of regulating metabolism and their transcriptional programmes is now apparent[35]. Movement of NAD^+ has been more specifically evaluated and the existence of a transporter able to flux NAD^+ to and from the mitochondria has been shown, although the identification of the responsible protein(s) remains unknown[36].

Conclusion

Our work shows although NAD^+ boosting has pharmacologic utility in maintaining metabolic health of skeletal muscle, the underlying REDOX status of the cell can be determinant of its impact. Here we find that adaptive upregulation of the NRK pathway is unproductive, yielding no increase in NAD^+ or NADH. Furthermore, attempts to exacerbate the H6KO model defective phenotype by ablating the NRK2 gene and producing a double knockout had no impact upon the skeletal muscle. This is supportive of the recent findings regarding the redundant nature of the NRKs, indicating NRK1 and NAMPT adaptive actions. Additionally, attempts to increase NAD^+ levels with acute intraperitoneal NR in the H6KO models were successful but had no significant impact over the physiology with many pathways failing to show a response differential from WT mice. Therefore, our work shows for the first time that NAD^+ biochemistry and the value of NAD^+ boosting as a strategy is dependent upon the metabolic context and REDOX stress environment within the target tissue. These being previously unidentified key determinants in the potential use of NAD^+ precursor compounds. Production of a double knockout of H6PD and NRK2 was successful at reducing total levels of skeletal muscle NAD(H) suggesting the existence REDOX influence over the cytosol and mitochondria that may impact metabolic functionality beyond the confined SR/ER environment.

List of Abbreviations

ER/SR: Endoplasmic/Sarcoplasmic Reticulum.

H6PD: Hexose-6-Phosphate Dehydrogenase.

NAD^+: Nicotinamide Adenine Dinucleotide.

NMN: Nicotinamide Mononucleotide.

NR: Nicotinamide Riboside.

NRK: Nicotinamide Riboside Kinase.

TA: Tibialis Anterior

SOL: Soleus

Author contributions

CLD and GGL conceived the study. CLD, GGL and DT wrote the manuscript. Experimental work was performed by CLD, AEZ, LOB, RSF, YH, DC, AG,DW, JA.

Conflicts of interest

None

Acknowledgements

We thank Chromadex (Irvine, California) for providing nicotinamide riboside.

Funding

This work was supported by a Wellcome Trust Senior Research Fellowship awarded to G.G.L. (GGL-104612/Z/14/Z).

Availability of data and materials

Datasets used in this study are available from the author upon request.

References

1 Semjonous, N. M. *et al.* Hexose-6-phosphate dehydrogenase contributes to skeletal muscle homeostasis independent of 11beta-hydroxysteroid dehydrogenase type 1. *Endocrinology* **152**, 93-102, doi:10.1210/en.2010-0957 (2011).

2 Marbet, P., Klusonova, P., Birk, J., Kratschmar, D. V. & Odermatt, A. Absence of hexose-6-phosphate dehydrogenase results in reduced overall glucose consumption but does not prevent 11beta-hydroxysteroid dehydrogenase-1-dependent glucocorticoid activation. *FEBS J* **285**, 3993-4004, doi:10.1111/febs.14642 (2018).

3 Belenky, P., Bogan, K. L. & Brenner, C. NAD+ metabolism in health and disease. *Trends Biochem Sci* **32**, 12-19, doi:10.1016/j.tibs.2006.11.006 (2007).

4 Bogan, K. L. & Brenner, C. Nicotinic acid, nicotinamide, and nicotinamide riboside: a molecular evaluation of NAD+ precursor vitamins in human nutrition. *Annu Rev Nutr* **28**, 115-130, doi:10.1146/annurev.nutr.28.061807.155443 (2008).

5 Schondorf, D. C. *et al.* The NAD+ Precursor Nicotinamide Riboside Rescues Mitochondrial Defects and Neuronal Loss in iPSC and Fly Models of Parkinson's Disease. *Cell Rep* **23**, 2976-2988, doi:10.1016/j.celrep.2018.05.009 (2018).

6 Hou, Y. *et al.* NAD(+) supplementation normalizes key Alzheimer's features and DNA damage responses in a new AD mouse model with introduced DNA repair deficiency. *Proceedings of the National Academy of Sciences of the United States of America* **115**, E1876-E1885, doi:10.1073/pnas.1718819115 (2018).

7 Diguet, N. *et al.* Nicotinamide Riboside Preserves Cardiac Function in a Mouse Model of Dilated Cardiomyopathy. *Circulation* **137**, 2256-2273, doi:10.1161/CIRCULATIONAHA.116.026099 (2018).

8 Fletcher, R. S. *et al.* Nicotinamide riboside kinases display redundancy in mediating nicotinamide mononucleotide and nicotinamide riboside metabolism in skeletal muscle cells. *Mol Metab* **6**, 819-832, doi:10.1016/j.molmet.2017.05.011 (2017).

9 Zhang, H. *et al.* NAD(+) repletion improves mitochondrial and stem cell function and enhances life span in mice. *Science* **352**, 1436-1443, doi:10.1126/science.aaf2693 (2016).

10 Ryu, D. *et al.* NAD+ repletion improves muscle function in muscular dystrophy and counters global PARylation. *Sci Transl Med* **8**, 361ra139, doi:10.1126/scitranslmed.aaf5504 (2016).

11 Canto, C., Menzies, K. J. & Auwerx, J. NAD(+) Metabolism and the Control of Energy Homeostasis: A Balancing Act between Mitochondria and the Nucleus. *Cell Metab* **22**, 31-53, doi:10.1016/j.cmet.2015.05.023 (2015).

12 Mouchiroud, L. *et al.* The NAD(+)/Sirtuin Pathway Modulates Longevity through Activation of Mitochondrial UPR and FOXO Signaling. *Cell* **154**, 430-441, doi:10.1016/j.cell.2013.06.016 (2013).

13 Canto, C. *et al.* The NAD(+) precursor nicotinamide riboside enhances oxidative metabolism and protects against high-fat diet-induced obesity. *Cell Metab* **15**, 838-847, doi:10.1016/j.cmet.2012.04.022 (2012).

14 Ratajczak, J. *et al.* NRK1 controls nicotinamide mononucleotide and nicotinamide riboside metabolism in mammalian cells. *Nat Commun* **7**, 13103, doi:10.1038/ncomms13103 (2016).

15 Lavery, G. G. *et al.* Hexose-6-phosphate dehydrogenase knock-out mice lack 11 beta-hydroxysteroid dehydrogenase type 1-mediated glucocorticoid generation. *The Journal of biological chemistry* **281**, 6546-6551, doi:10.1074/jbc.M512635200 (2006).

16 Lavery, G. G. *et al.* Hypoglycemia with enhanced hepatic glycogen synthesis in recombinant mice lacking hexose-6-phosphate dehydrogenase. *Endocrinology* **148**, 6100-6106, doi:10.1210/en.2007-0963 (2007).

17 Bujalska, I. J. *et al.* Lack of hexose-6-phosphate dehydrogenase impairs lipid mobilization from mouse adipose tissue. *Endocrinology* **149**, 2584-2591, doi:10.1210/en.2007-1705 (2008).

18 Lavery, G. G. *et al.* Deletion of hexose-6-phosphate dehydrogenase activates the unfolded protein response pathway and induces skeletal myopathy. *The Journal of biological chemistry* **283**, 8453-8461, doi:10.1074/jbc.M710067200 (2008).
19 Xia, J., Sinelnikov, I. V., Han, B. & Wishart, D. S. MetaboAnalyst 3.0--making metabolomics more meaningful. *Nucleic Acids Res* **43**, W251-257, doi:10.1093/nar/gkv380 (2015).
20 Xia, J. & Wishart, D. S. Web-based inference of biological patterns, functions and pathways from metabolomic data using MetaboAnalyst. *Nat Protoc* **6**, 743-760, doi:10.1038/nprot.2011.319 (2011).
21 Tserng, K. Y., Jin, S. J., Kerr, D. S. & Hoppel, C. L. Urinary 3-hydroxydicarboxylic acids in pathophysiology of metabolic disorders with dicarboxylic aciduria. *Metabolism* **40**, 676-682 (1991).
22 Bergoffen, J., Kaplan, P., Hale, D. E., Bennett, M. J. & Berry, G. T. Marked elevation of urinary 3-hydroxydecanedioic acid in a malnourished infant with glycogen storage disease, mimicking long-chain L-3-hydroxyacyl-CoA dehydrogenase deficiency. *J Inherit Metab Dis* **16**, 851-856 (1993).
23 Strauss, A. W. *et al.* Molecular basis of human mitochondrial very-long-chain acyl-CoA dehydrogenase deficiency causing cardiomyopathy and sudden death in childhood. *Proceedings of the National Academy of Sciences of the United States of America* **92**, 10496-10500 (1995).
24 Oakey, L. A. *et al.* Metabolic tracing reveals novel adaptations to skeletal muscle cell energy production pathways in response to NAD (+) depletion. *Wellcome Open Res* **3**, 147, doi:10.12688/wellcomeopenres.14898.1 (2018).
25 Deloux, R., Tannous, C., Ferry, A., Li, Z. & Mericskay, M. Aged Nicotinamide Riboside Kinase 2 Deficient Mice Present an Altered Response to Endurance Exercise Training. *Front Physiol* **9**, 1290, doi:10.3389/fphys.2018.01290 (2018).
26 Tarrago, M. G. *et al.* A Potent and Specific CD38 Inhibitor Ameliorates Age-Related Metabolic Dysfunction by Reversing Tissue NAD(+) Decline. *Cell metabolism* **27**, 1081-1095 e1010, doi:10.1016/j.cmet.2018.03.016 (2018).
27 Agerholm, M. *et al.* Perturbations of NAD(+) salvage systems impact mitochondrial function and energy homeostasis in mouse myoblasts and intact skeletal muscle. *Am J Physiol Endocrinol Metab* **314**, E377-E395, doi:10.1152/ajpendo.00213.2017 (2018).
28 Uddin, G. M., Youngson, N. A., Sinclair, D. A. & Morris, M. J. Head to Head Comparison of Short-Term Treatment with the NAD(+) Precursor Nicotinamide Mononucleotide (NMN) and 6 Weeks of Exercise in Obese Female Mice. *Front Pharmacol* **7**, 258, doi:10.3389/fphar.2016.00258 (2016).
29 Frederick, D. W. *et al.* Loss of NAD Homeostasis Leads to Progressive and Reversible Degeneration of Skeletal Muscle. *Cell metabolism* **24**, 269-282, doi:10.1016/j.cmet.2016.07.005 (2016).
30 Tsachaki, M., Mladenovic, N., Stambergova, H., Birk, J. & Odermatt, A. Hexose-6-phosphate dehydrogenase controls cancer cell proliferation and migration through pleiotropic effects on the unfolded-protein response, calcium homeostasis, and redox balance. *FASEB J* **32**, 2690-2705, doi:10.1096/fj.201700870RR (2018).
31 Knezevic, C. E. *et al.* Proteome-wide Profiling of Clinical PARP Inhibitors Reveals Compound-Specific Secondary Targets. *Cell Chem Biol* **23**, 1490-1503, doi:10.1016/j.chembiol.2016.10.011 (2016).
32 Palermo, A. T. *et al.* Transcriptional response to GAA deficiency (Pompe disease) in infantile-onset patients. *Mol Genet Metab* **106**, 287-300, doi:10.1016/j.ymgme.2012.05.004 (2012).
33 Goody, M. F. *et al.* NAD+ biosynthesis ameliorates a zebrafish model of muscular dystrophy. *PLoS Biol* **10**, e1001409, doi:10.1371/journal.pbio.1001409 (2012).
34 Ferreira, C. R. & Gahl, W. A. Lysosomal storage diseases. *Transl Sci Rare Dis* **2**, 1-71, doi:10.3233/TRD-160005 (2017).

35 Ryu, K. W. *et al.* Metabolic regulation of transcription through compartmentalized NAD(+) biosynthesis. *Science* **360**, doi:10.1126/science.aan5780 (2018).
36 Davila, A. *et al.* Nicotinamide adenine dinucleotide is transported into mammalian mitochondria. *Elife* **7**, doi:10.7554/eLife.33246 (2018).

Figure legends

Figure 1. Unbiased identification of metabolic shifts supported by transcriptional changes. (A) Pathways analysis of unbiased metabolomics from WT (n=3) and H6KO (n=3) Tibialis Anterior Skeletal Muscle. (B) Numerical output from pathway analysis of WT and H6PDH KO Tibialis Anterior Skeletal Muscle. Values shown are original value from pathway analysis. (C-F) Quantification of NAD+, NADH and total NAD(H) in WT (n=7) and H6KO (n=6) TA muscle. (G) Schematic representation of the biosynthetic generation of NAD from nicotinamide Riboside (NR) and nicotinamide (NAM) salvage, enzymes shown in red. (H) qRT-PCR of NAD+ synthesis and salvage genes in WT (n=7) and H6KO (n=7) TA. (I+J) Immunoblots and quantification of WT (n=9) and H6KO (n=9) TA lysates. *P<0.05, **P<0.01 and ***P<0.001.

Figure 2. Impaired mitochondrial fatty acid oxidation in skeletal muscle due to H6 KO. (A) High resolution respirometry of fatty acid oxidation in permeabilised Tibialis Anterior WT (n=3) in and H6KO (n=3). (B) High resolution respirometry of fatty acid oxidation using WT (n=3) and H6KO (n=3) permeabilised Soleus. (C) Mitochondrial DNA (mtDNA) quantification of WT (n=7) and H6KO (n=7) muscle, measured using qRT-PCR. (D) Immunoblots WT and H6KO protein lysates (n=9) probed for oxidative phosphorylation enzyme subunit abundance. (E) Acylcarnitine species levels in WT (n=9) and H6KO (n=11) muscle measured using GC-MS/MS. Data expressed as heat-maps with z-score values representing metabolite abundance in WT and H6KO. Box and Whisker plots showing significantly altered short acylcarnitines. (F) qRT-PCR measurement of genes critical carnitine and fatty acids metabolism in WT (n=7) and H6KO (n=7) TA. (G) Schematic showing carnitine and fatty acid metabolism between cytosol and mitochondria. (H) Immunoblots of acetylated proteins within WT (n=6) and H6KO (n=6) skeletal muscle. *P<0.05, **P<0.01 and ***P<0.001.

Figure 3. H6 KO upregulates the muscle specific metabolic pathway regulating NAD(H) salvage and biosynthesis. (A-D) NAD^+, NAD(H) and total NAD(H) quantification in skeletal muscle of WT and H6KO +/- intraperitoneal (i.p.) Nicotinamide Riboside (NR) (n=6-9). (E) qRT-PCR data of genes involved in the biosynthesis of NAD+ and salvage of NAM in WT and H6KO muscle +/- i.p. NR (n=6-9). (F) qRT-PCR data of genes critical carnitine and fatty acids metabolism in WT and H6KO muscle +/- i.p. NR (n=6-9). (G-H) Immunoblots and quantification of the NAM salvage protein NAMPT and the skeletal muscle specific protein NRK2 (n=6). (I) High resolution respirometry of fatty acid oxidation in permeabilised Tibialis Anterior WT in and H6KO i.p NR (n=3). (I) High resolution respiration for fatty acid oxidation using WT and H6KO after i.p NR permeabilised Soleus (n=3). (J) Immunoblots showing ER stress regulator CHOP and protein folding factors PDI and ERO1a in WT and H6KO +/- i.p NR. (K) Immunoblots showing total lysine acetylation and IDH acetylation in WT and H6KO muscle +/- i.p NR. (n=6-9). *P<0.05, **P<0.01 and ***P<0.001.

Figure 4. Double Knockout of H6PDH and NRK2 reduces NAD^+ in skeletal muscle independently of mitochondrial FAO and REDOX status. (A-D) NAD^+, NADH and total NAD(H) levels in WT, H6KO, NRK2KO and DKO (H6KO-NRK2KO) TA muscle (n=3-6). (E-G) Skeletal muscle tissue weights from WT, H6KO, NRK2KO and H6-NRK2 Double Knockout (DKO) (n=3-6). (H) qRT-PCR of NAD^+ biosynthetic gene expression in WT, H6KO, NRK2 KO and DKO TA (n=3-6). (I) qRT-PCR of mitochondrial and Acyl-CoA genes in TA of WT, H6KO, NRK2 KO and DKO (n=3-6). (J) qRT-PCR of ER/SR stress response genes in WT, H6KO, NRK2KO and DKO TA (n=3-6). (F-K) Immunoblots of CHOP and protein folding factors PDI and ERO1a in WT, H6KO, NRK2 KO and DKO muscle lysates (n=3-6). (L) Immunoblots of total lysine acetylation, IDH2 acetylation in WT, H6KO, NRK2KO and DKO muscle protein lysates (n=3-6). *P<0.05, **P<0.01 and ***P<0.001.

Supplementary Figure 1. Targeted metabolomics of WT and H6KO Muscle, Serum and Liver (n=9-11).

Supplementary Figure 2. Metabolic impact of H6PD deficiency upon the skeletal muscle. (A-D) Metabolomic assessment of WT and H6KO Tibialis Anterior measured by LC-MS. (A) Metabolomics analysis of WT (n=9) and H6PDH KO (n=11) Tiabialis Anterior Skeletal Muscle. Data expressed as boxplots representing abundance. (A-D) Box and Whisker plot showing selected (A) Lysophospholipids, (B) Phosphotidylcholines, (C) Amino acids and (D) Sphingomyelins quantification from WT and H6KO TA. Error bars represent minimum and maximum values. *$p<0.05$, **$p<0.01$, ***$p<0.001$. two-tailed unpaired Students t-test. (C)

Supplementary Table 1. Unbiased metabolite abundance in H6KO and WT skeletal muscle. (A) Metabolomic assessment of WT (n=3) and H6KO (n=3) Tibialis Anterior measured by LC-MS. Shown in table 1 are the most differentially abundant metabolites in H6KO muscle compared to WT.

Fig 1.

A.

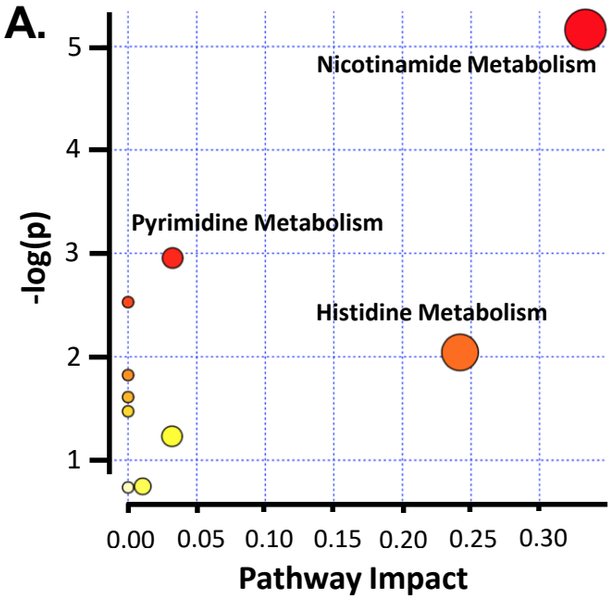

B.

Metabolic Pathway	Total	Expected	Hits	Raw p
Nicotinamide Metabolism	13	0.12	2	5.73E-03
Pyrimidine Metabolism	41	0.38	2	5.21E-02
Nitrogen Metabolism	9	0.08	1	7.98E-02
Histidine Metabolism	15	0.14	1	1.30E-01
Pentose Phosphate Pathway	19	0.17	1	1.62E-01
Alanine, Aspartate and Glutamate Metabolism	24	0.22	1	2.00E-01
Inositol Phosphate Metabolism	28	0.26	1	2.29E-01
Amino Sugar and Nucleotide Sugar Metabolism	37	0.34	1	2.92E-01
Purine Metabolism	68	0.62	1	4.74E-01
Aminoacyl-tRNA Biosynthesis	69	0.63	1	4.79E-01

C.

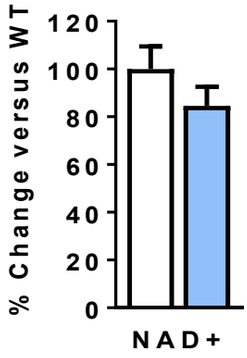

D.

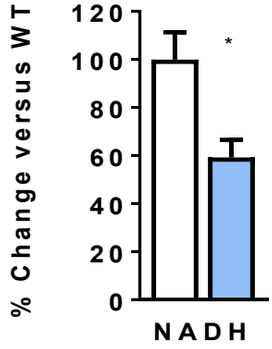

E.

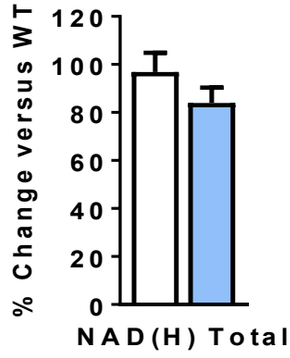

F.

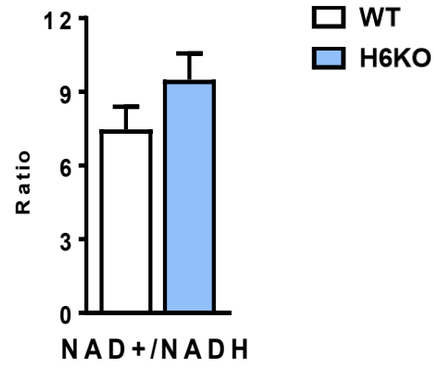

G.

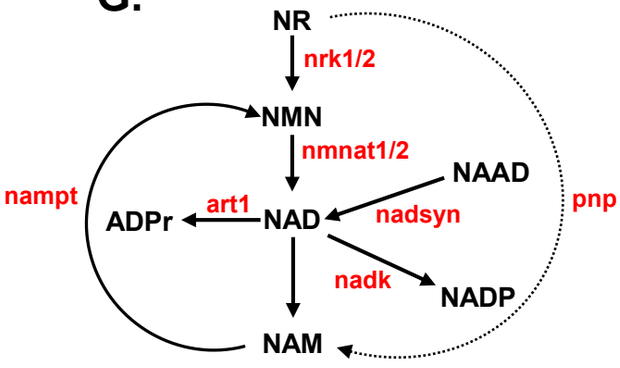

H.

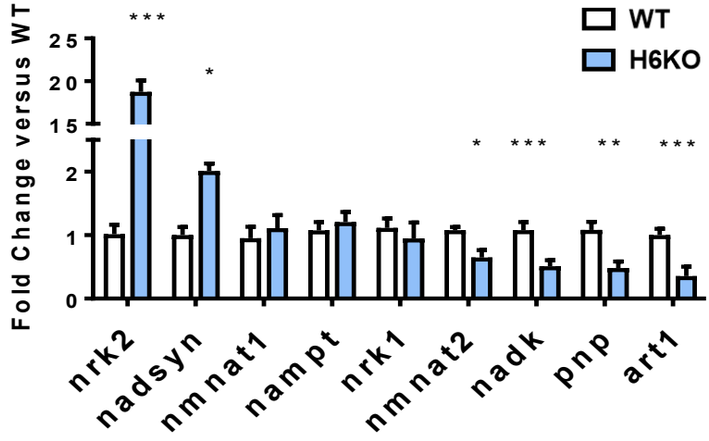

I.

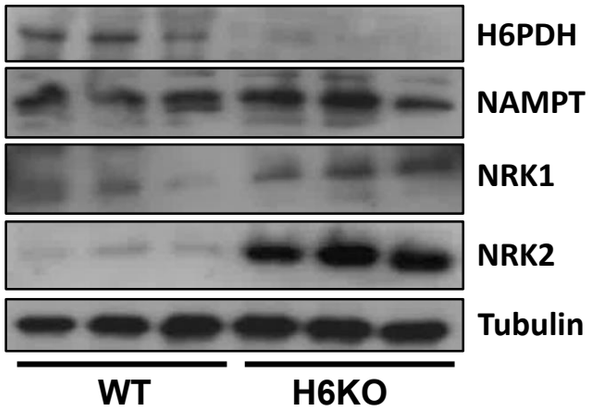

J.

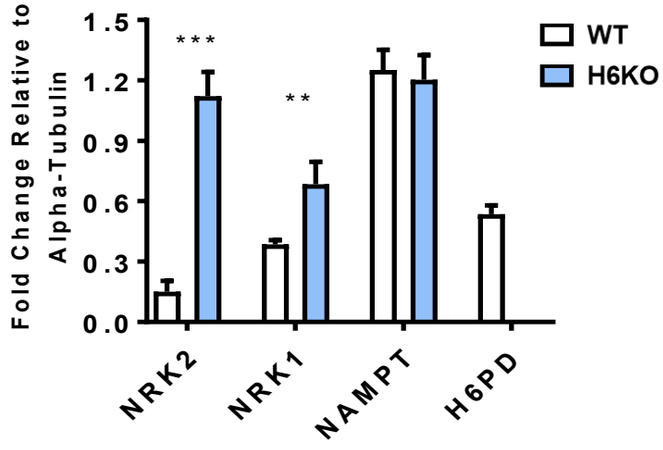

Fig 2.

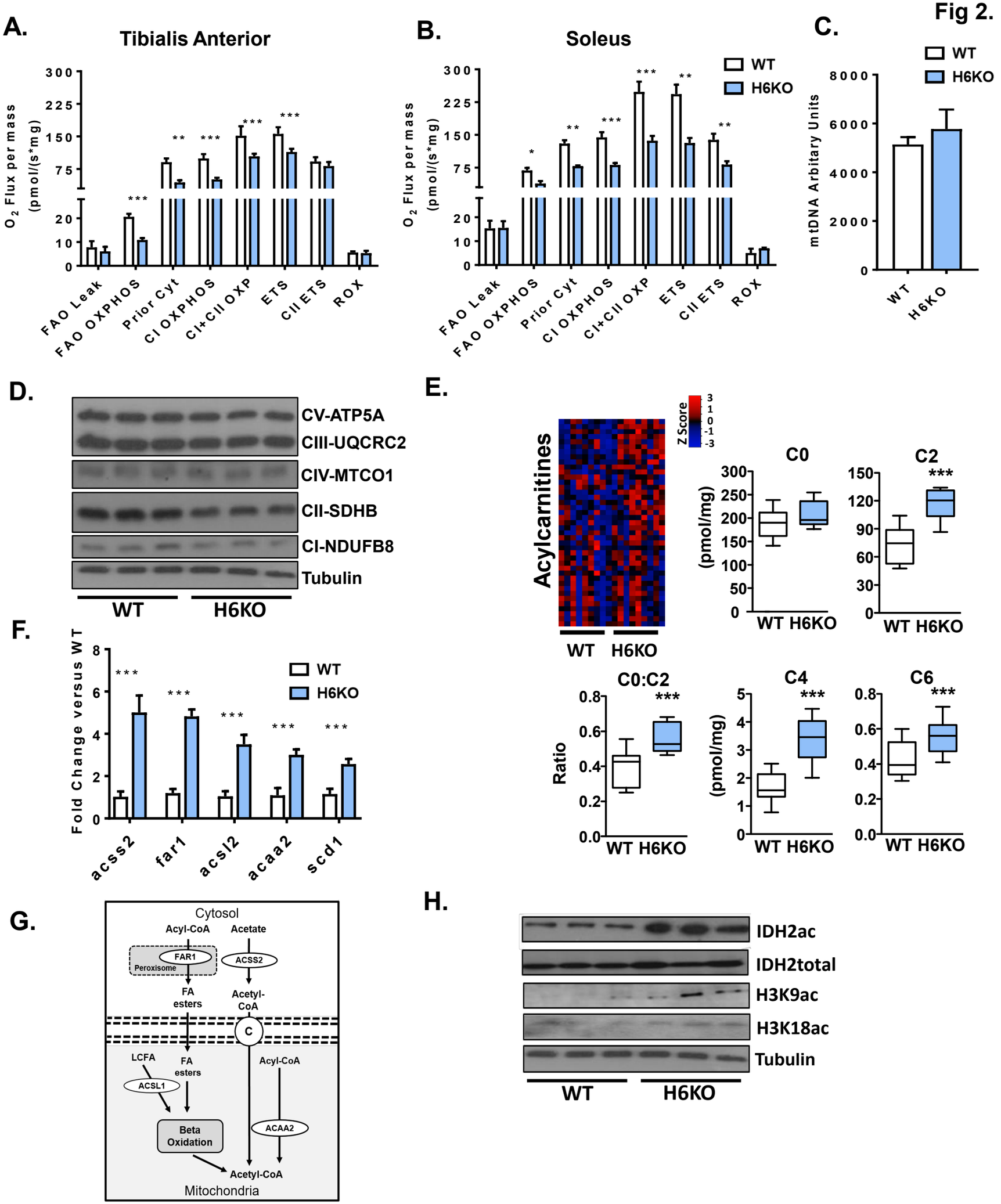
A.
Tibialis Anterior
B.
Soleus
C.
WT
H6KO
O2 Flux per mass (pmol/(s*mg)
mtDNA Arbitary Units
FAO Leak
FAO OXPHOS
Prior Cyt
CI OXPHOS
CI+CII OXP
ETS
CII ETS
ROX
D.
CV-ATP5A
CIII-UQCRC2
CIV-MTCO1
CII-SDHB
CI-NDUFB8
Tubulin
E.
Acylcarnitines
Z Score
C0
C2
C0:C2
C4
C6
(pmol/mg)
Ratio
F.
Fold Change versus WT
acss2
far1
acsl2
acaa2
scd1
G.
Cytosol
Acyl-CoA
Acetate
FAR1
Peroxisome
ACSS2
FA esters
Acetyl-CoA
C
LCFA
ACSL1
Beta Oxidation
ACAA2
Mitochondria
H.
IDH2ac
IDH2total
H3K9ac
H3K18ac
Tubulin

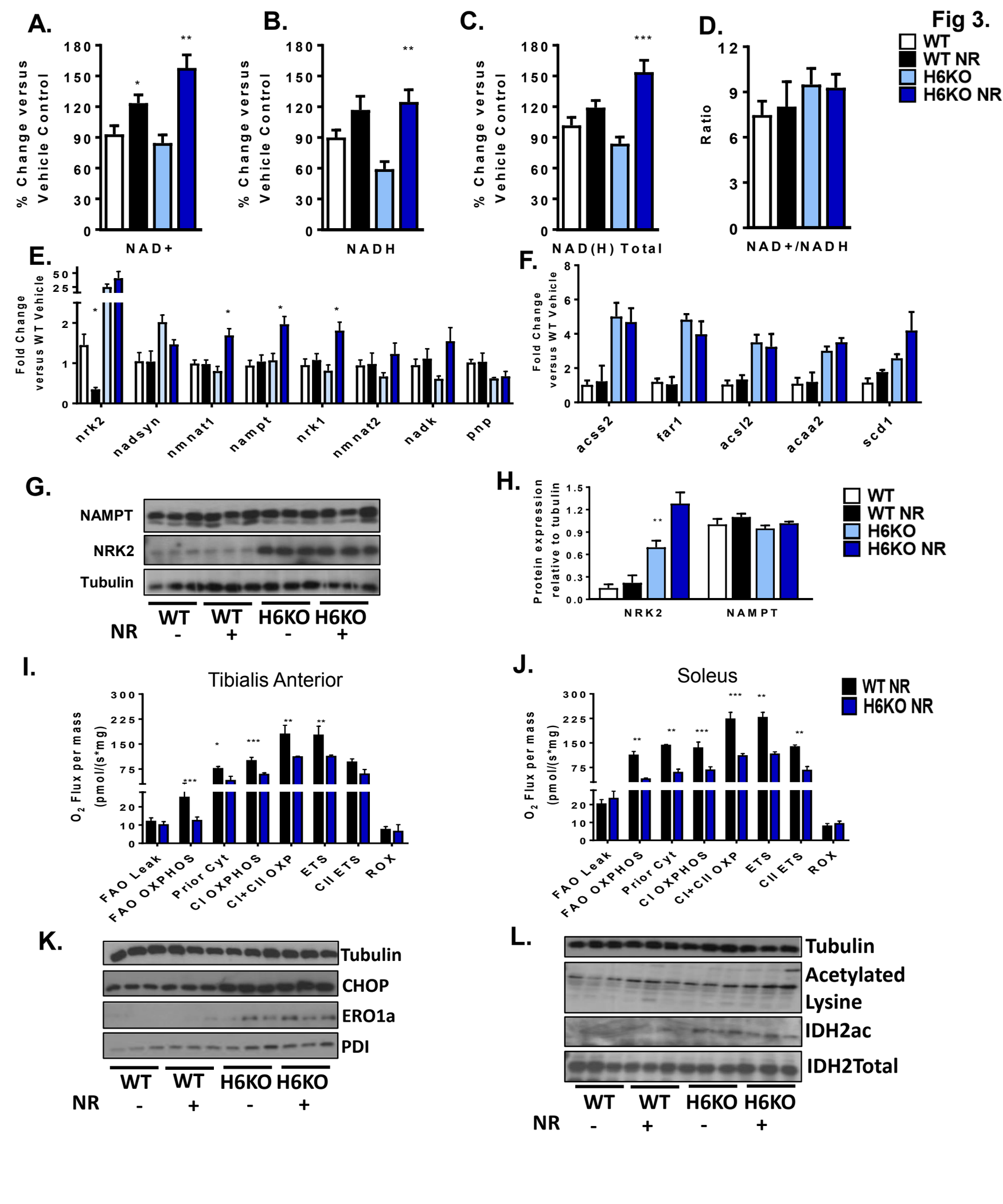
Fig 3.
A.
B.
C.
D.
% Change versus Vehicle Control
NAD+
NADH
NAD(H) Total
Ratio
NAD+/NADH
WT
WT NR
H6KO
H6KO NR
E.
Fold Change versus WT Vehicle
nrk2
nadsyn
nmnat1
nampt
nrk1
nmnat2
nadk
pnp
F.
acss2
far1
acsl2
acaa2
scd1
G.
NAMPT
NRK2
Tubulin
WT
WT
H6KO
H6KO
NR
-
+
-
+
H.
Protein expression relative to tubulin
NRK2
NAMPT
I.
Tibialis Anterior
O2 Flux per mass (pmol/(s*mg)
FAO Leak
FAO OXPHOS
Prior Cyt
CI OXPHOS
CI+CII OXP
ETS
CII ETS
ROX
J.
Soleus
K.
Tubulin
CHOP
ERO1a
PDI
L.
Tubulin
Acetylated Lysine
IDH2ac
IDH2Total

Fig 4.

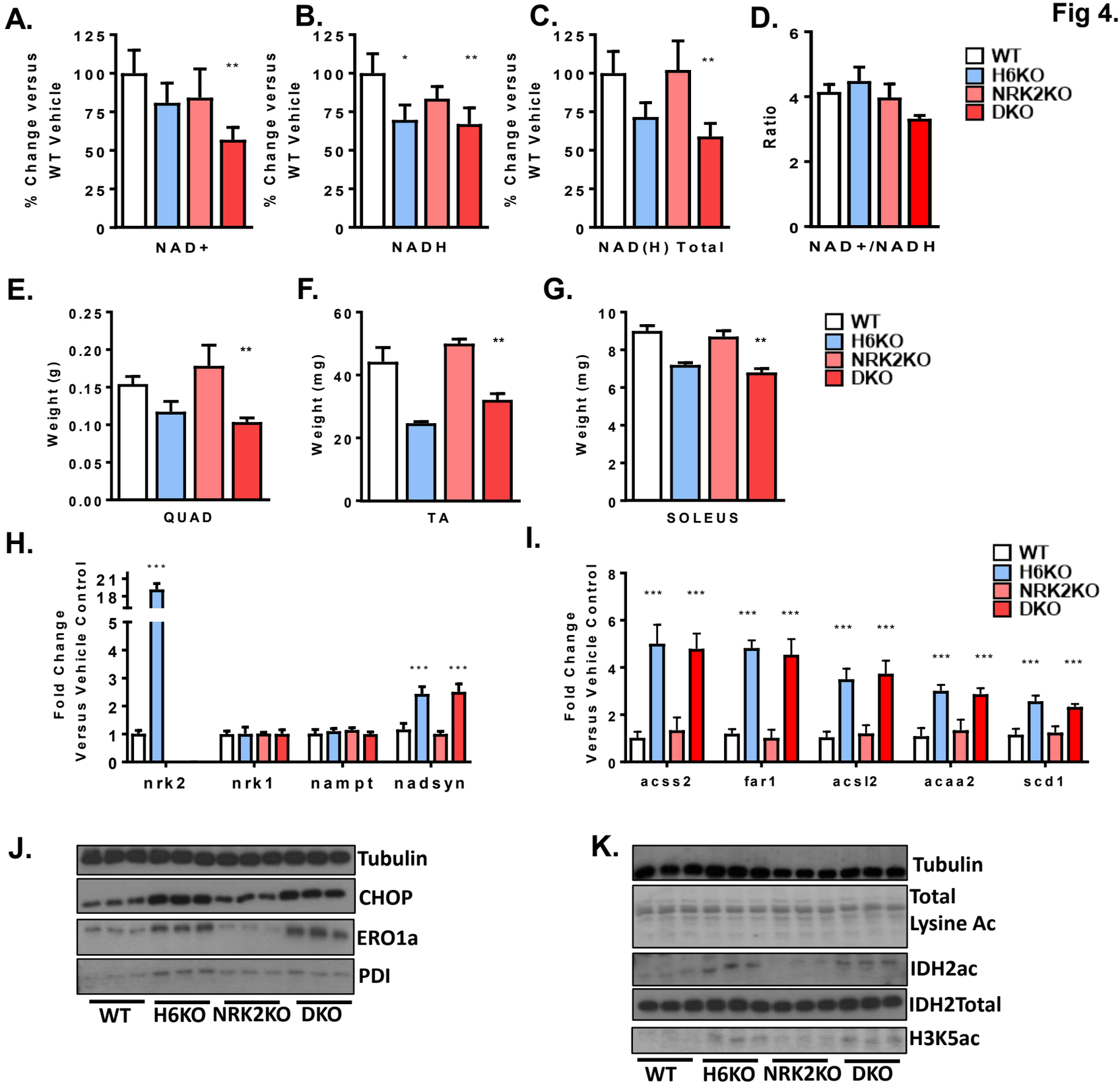
A.
% Change versus WT Vehicle
NAD+
B.
NADH
C.
NAD(H) Total
D.
Ratio
NAD+/NADH
WT
H6KO
NRK2KO
DKO
E.
Weight (g)
QUAD
F.
Weight (mg)
TA
G.
SOLEUS
H.
Fold Change Versus Vehicle Control
nrk2
nrk1
nampt
nadsyn
I.
acss2
far1
acsl2
acaa2
scd1
J.
Tubulin
CHOP
ERO1a
PDI
K.
Total Lysine Ac
IDH2ac
IDH2Total
H3K5ac

Supplementary Fig 1

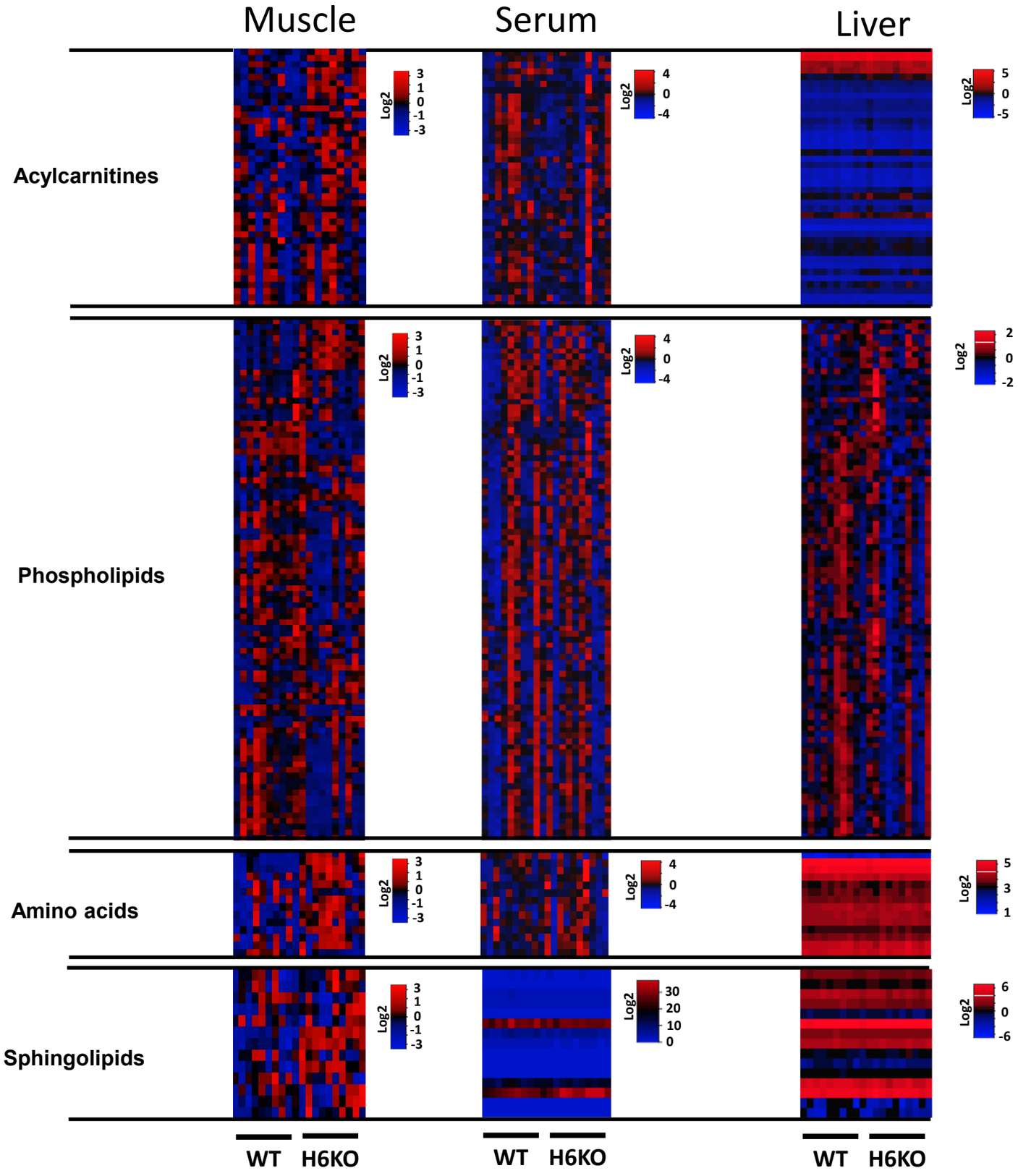

Supplementary Fig 2

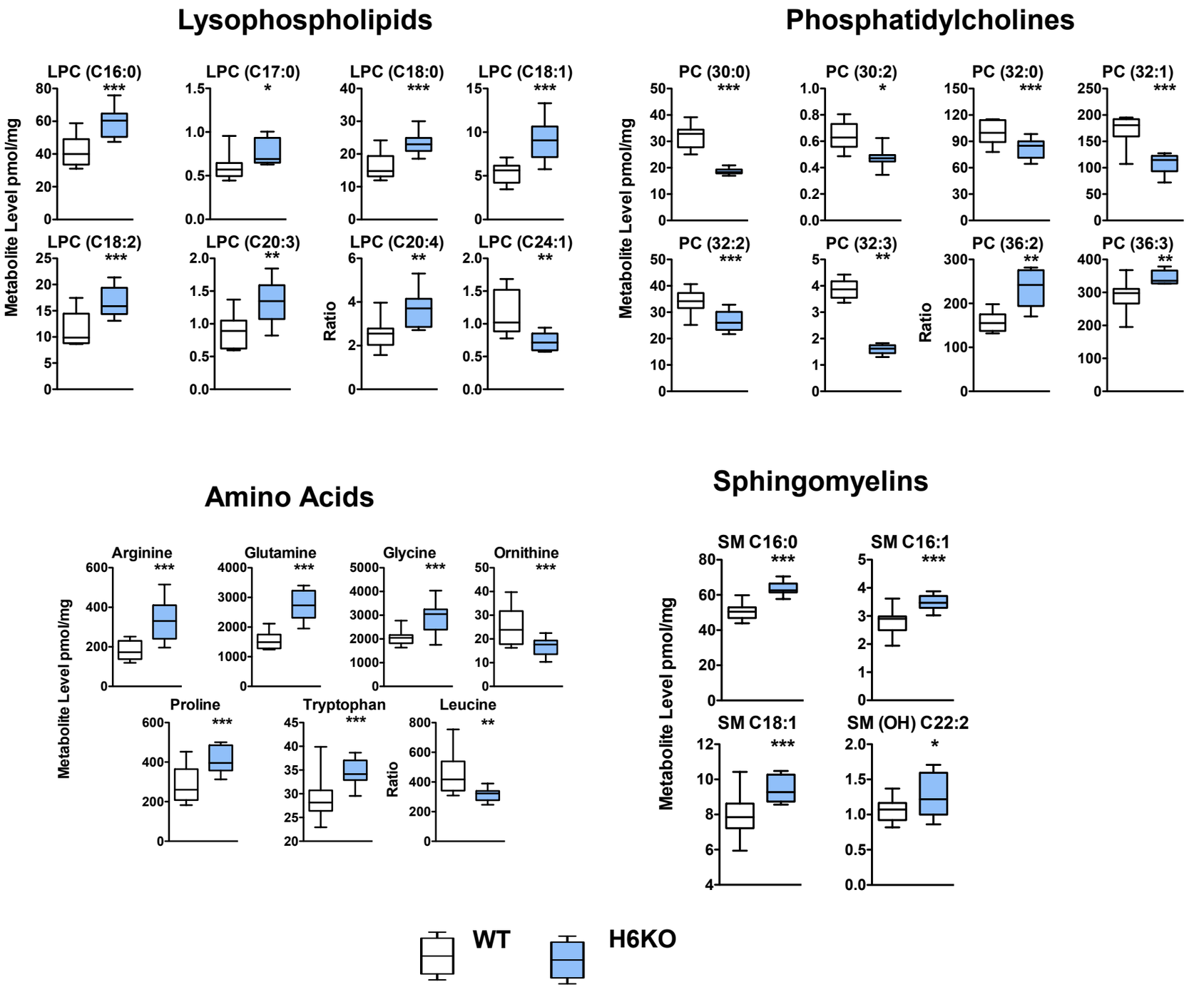

Supplementary Table 1

Compound Differentially Abundant in H6KO Compared to WT muscle	p
N6,N6,N6-Trimethyl-L-lysine	4.41E-04
L-Methionine S-oxide	3.94E-03
3-Hydroxysebacicacid	7.25E-03
4-Aminobutanoate	7.71E-03
2,3,4-trihydroxy-butanoic acid	9.10E-03
Leu-Gln-Pro	1.08E-02
1H-Imidazole-4-ethanamine	1.13E-02
(R)-1-Aminopropan-2-ol	1.19E-02
2',6'-Dihydroxy-4'-methoxy-3'-prenyldihydrochalcone	1.20E-02
Leu-Pro	1.33E-02
NAD+	1.67E-02
L-rhamnitol	1.92E-02
L-Proline	1.93E-02
N-Undecanoylglycine	1.96E-02
L-Valine	2.01E-02
cis-5-Tetradecenoylcarnitine	2.02E-02
2,3,4-trihydroxy-butanoic acid	2.12E-02
Creatinine	2.46E-02
Citrate	3.03E-02
4-Aminobutanoate	3.11E-02
PE (18:0/20:4 (5Z,8Z,11Z,14Z))	3.25E-02
4-Aminobutanoate	3.28E-02
N,N,N-Trimethylserotonin	3.36E-02
Dethiobiotin	3.68E-02
1-Methylnicotinamide	3.97E-02
D-Glucosamine 6-phosphate	4.24E-02
Tetradecanoylcarnitine	4.38E-02
GMP	4.43E-02
O-Butanoylcarnitine	4.43E-02
Choline phosphate	4.54E-02
D-Glucose 6-phosphate	4.79E-02